Chinese Chemical Letters 36 (2025) 110348

Contents lists available at ScienceDirect

Chinese Chemical Letters

journal homepage: www.elsevier.com/locate/cclet

Mn(II) enhanced permanganate oxidation of trace organic pollutants in water: Critical role of *in situ* formation of colloidal MnO_2

Haoting Wang[a,b], Mengfan Luo[a,b], Yuzhong Wang[c], Jialong Yin[a,b], Heng Zhang[a,b,*], Jia Zhao[a,b], Bo Lai[a,b,d]

[a] State Key Laboratory of Hydraulics and Mountain River Engineering, College of Architecture and Environment, Sichuan University, Chengdu 610065, China
[b] Sino-German Centre for Water and Health Research, Sichuan University, Chengdu 610065, China
[c] Downhole Technology Service Company, Bohai Drilling Engineering Company, Ltd., CNPC, Tianjin 300283, China
[d] Key Laboratory of Jiangxi Province for Persistent Pollutants Prevention Control and Resource Reuse, Nanchang Hangkong University, Nanchang 330063, China

ARTICLE INFO

Article history:
Received 6 July 2024
Revised 15 August 2024
Accepted 16 August 2024
Available online 17 August 2024

Keywords:
Permanganate
Mn(II)
Sulfamethoxazole
MnO_2
Autocatalysis

ABSTRACT

Studies widely acknowledge the enhancement of permanganate (Mn(VII)) oxidation of organic contaminants by coexisting matrices in water. This study investigated the positive influence of Mn(II), a common soluble metal ion, on the removal of trace organic pollutants by Mn(VII). Results showed that introducing 20 μmol/L Mn(II) at pH 5.0 accelerated trace organic pollutant removal by promoting colloidal MnO_2 formation. UV−vis spectrum, quenching, and probe experiments confirmed role of MnO_2 in sulfamethoxazole (SMX) oxidation, with Mn(III) playing a predominant role. Meanwhile, *in situ*-generated MnO_2 facilitated Mn(VII)* formation, enhancing oxidation performance, as indicated by Raman spectroscopy and electrochemical analysis. Eleven transformation products (TPs) of SMX in the Mn(VII)/Mn(II) process were detected by UPLC-QTOF-MS/MS. Subsequently, the reaction pathways of SMX were elucidated through Fukui index analysis and the identification of TPs. Additionally, toxicity simulations with Toxicity Estimation Software Tool (T.E.S.T.) software revealed significantly lower cytotoxicity of TPs of SMX compared to the parent compound. This study unveils an effective strategy to enhance Mn(VII)-mediated degradation of organic pollutants in water, elucidating Mn(II)-induced Mn(VII) activation mechanisms.

Trace organic pollutants, including antibiotics and endocrine disruptors, present considerable threats to human health, microbial communities, and ecosystems [1,2]. Traditional techniques, like adsorption and biodegradation, are not successful in reducing these pollutants in wastewater [3,4]. Advanced oxidation processes (AOPs), such as Fenton-like technology and photocatalytic technology, are a cutting-edge method in water purification that targets refractory organic contaminants with highly reactive species [5-9]. However, radicals have short lifespans, are easily quenched, and coexisting matrices pose significant challenges [10,11].

Permanganate (Mn(VII)) oxidation has gained attention for its effective removal of organic pollutants due to its stability, cost-effectiveness, and environmentally friendly by-products [4,12,13]. Studies highlight that natural water components such as humic acid, oxyanions, and soluble metal ions enhance pollutant degradation by Mn(VII) [14-16]. Mechanisms include the formation of reactive manganese species (RMnS) like Mn(VI), Mn(V), and MnO_2, which are highly reactive towards pollutants, and the oxyanion-stabilized MnO_2 catalytic activity enhancement. These findings underscore the role of *in situ*-generated colloidal MnO_2.

Mn(II) is widely present in natural water bodies, often even exceeding 0.3 mg/L and affecting water odor [17]. Mn(VII) is widely used to remove Mn(II) through *in situ* oxidation and coagulation, rapidly forming MnO_2 nanoparticles that can be easily removed by conventional methods. Interestingly, excessive Mn(II) not only does not inhibit but enhances the degradation of organic pollutants by Mn(VII) [18,19]. However, the specific mechanism of Mn(II) enhancing the oxidative efficiency of Mn(VII) remains unclear.

This study aims to investigate how Mn(II) activates Mn(VII) to degrade organic pollutants, focusing on sulfamethoxazole (SMX). The effects of Mn(VII) dosage, Mn(II) dosage, and pH on pollutant removal will be discussed. The research will also explore the primary species in the Mn(VII)/Mn(II) system, especially MnO_2, through quenching experiments and characterization. Additionally, it will identify the products and pathways of SMX oxidation by Mn(VII)/Mn(II) and analyze their cytotoxicity. The goal is to elu-

* Corresponding author.
E-mail address: zhangheng01@scu.edu.cn (H. Zhang).

https://doi.org/10.1016/j.cclet.2024.110348
1001-8417/

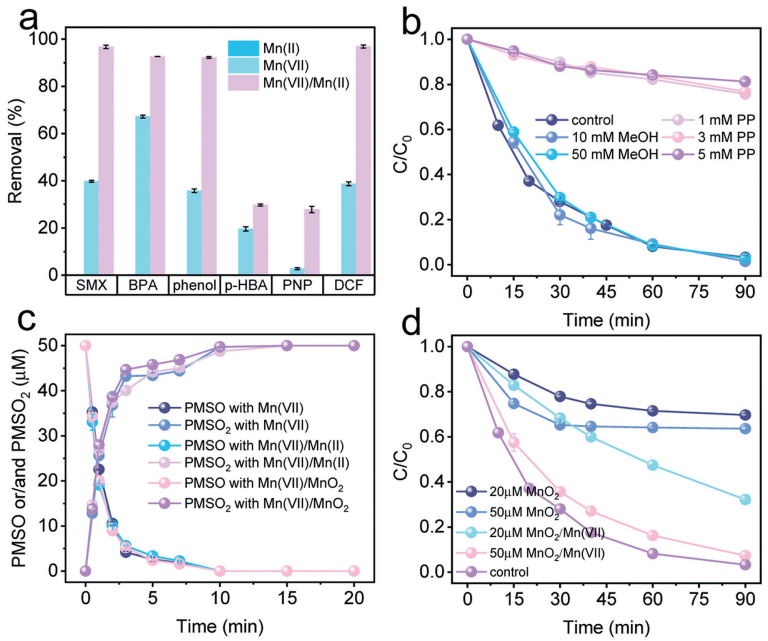

Fig. 1. (a) Effect of Mn(II) on SMX, BPA, phenol, *p*-HBA, PNP, and DCF removal by Mn(VII). Reaction time is 90, 20, 45, 90, 90, and 7 min for SMX, BPA, phenol, *p*-HBA, PNP, and DCF, respectively. (b) Influence of MeOH and PP on SMX degradation. (c) Concentrations change of PMSO and $PMSO_2$ in different process $[MnO_2] = 20\,\mu mol/L$. (d) Contributions of MnO_2 on SMX removal. Experimental conditions: [Mn(VII)] = 150 μmol/L, [Mn(II)] = 20 μmol/L, [SMX] = [BPA] = [phenol] = [*p*-HBA] = [PNP] = [DCF] = 5 μmol/L, [PMSO] = 50 μmol/L, pH 5.0. mM: mmol/L, μM: μmol/L.

cidate the Mn(II)-induced activation mechanism of Mn(VII), highlighting the potential of the Mn(VII)/Mn(II) system for treating organic pollutants in water.

The detailed information about the chemicals is provided in Text S1 (Supporting information).

A 100 mL reaction mixture was stirred at 550 rpm in a 200 mL glass beaker at 25 ± 1 °C. The pH was maintained at 4.0, 5.0, 6.0, or 7.0 using a 10 mmol/L acetate buffer. Initially, the selected organic pollutant (5 μmol/L) was mixed with water and buffer. Mn(VII) and Mn(II) were then added to start the reaction. Methanol (MeOH) was used to quench •OH and high-valent manganese, and potassium pyrophosphate (PP) stabilized Mn(III) for identification. At regular intervals, 0.5 mL of the solution was filtered by a polytetrafluoroethylene membrane (0.22 μm) and quenched with 20 μL of hydroxylamine hydrochloride (0.5 mol/L) for further analysis. All procedures were repeated in duplicate for accuracy.

The supporting information includes details of the high-performance liquid chromatography (HPLC, SHIMAZU) conditions (Table S1 in Supporting information), analytical methods for X-ray photoelectron spectroscopy (XPS), electron paramagnetic resonance (EPR) spectroscopy, Raman spectrum (Text S2 in Supporting information), the electrochemical system (Text S3 in Supporting information), and ultra-performance liquid chromatography quadrupole time-of-flight mass spectrometry (UPLC-QTOF-MS/MS, Agilent 6500) (Text S4 in Supporting information). Density functional theory calculations are conducted using the Gaussian 16 program package and program Multiwfn packages, the details are listed in Text S5 (Supporting information) [20,21].

The efficacy of Mn(II), Mn(VII) and Mn(VII)/Mn(II) systems in the elimination of six organic pollutants, including SMX, bisphenol A (BPA), phenol, *p*-hydroxybenzoic acid (*p*-HBA), *p*-nitrophenol (PNP) and sodium diclofenac (DCF), was assessed to confirm the impact of Mn(II) on Mn(VII) oxidation (Fig. 1a and Fig. S1 in Supporting information). The *pseudo*-first-order rate constants for the reactions among six organic pollutants were also obtained (Fig. S2 in Supporting information). These observations revealed that Mn(II) lacked the oxidative capability to remove organic pollutants, whereas the Mn(VII)/Mn(II) system showed significantly greater efficiency in removing all examined pollutants compared to the Mn(VII) alone system. This occurrence could be explained by the formation of reactive species within the Mn(VII)/Mn(II) system, enabling swift and efficient pollutant degradation. As SMX demonstrated a remarkable improvement in degradation, it was selected as the example pollutant.

Investigating the influence of parameters is crucial for optimizing reaction conditions. Fig. S3a (Supporting information) showed that increasing Mn(VII) dosage from 20 μmol/L to 250 μmol/L boosted SMX removal from 40% to 100%. Similarly, Fig. S3b (Supporting information) showed enhanced SMX degradation with higher initial Mn(II) concentrations, increasing from 40% to 100% as Mn(II) rose from 0 to 30 μmol/L. This improvement may be attributed to Mn(II) rapidly consuming Mn(VII) to form more reactive species, potentially accelerating SMX oxidation. Previous studies have indicated that RMnS play a critical role in the Mn(VII) oxidation of contaminants [22]. The impact of initial pH (4.0–7.0) on SMX degradation in Mn(VII)/Mn(II) systems is depicted in Fig. S3c (Supporting information), where degradation efficiency remained similar at pH 4.0 and 5.0 but decreased notably at pH 6.0 and 7.0. This trend likely stemmed from the enhanced oxidative potential of Mn(VII) under acidic conditions, while the reactivity of Mn(II) and Mn(VII) diminishes as pH rises.

MeOH, chosen for its quenching capability against hydroxyl radicals (•OH) ($k_{MeOH/•OH} = 9.7 \times 10^8$ L mol^{-1} s^{-1}) in the Mn(VII)/Mn(II) system [23], showed minimal impact on SMX degradation with 10 mmol/L and 50 mmol/L additions, indicating negligible •OH generation (Fig. 1b) [24]. Benzoic acid, a •OH probe to form the characteristic product *p*-HBA, similarly showed insignificant degradation in the Mn(VII)/Mn(II) system, supporting the absence of •OH radicals (Fig. S4 in Supporting information). To further investigate the generation of singlet oxygen ($^1O_2$) in the system, EPR technique were conducted using 2,2,6,6-tetramethylpiperidine (TEMP) as a spin trap. As shown in Fig. S5 (Supporting information), no characteristic signal was observed, indicating that $^1O_2$ was not produced in the system.

Previous studies have highlighted RMnS (Mn(III), MnO_2, Mn(V), Mn(VI)) as crucial in oxidizing organic contaminants [25]. Recent investigations using PMSO as a chemical probe revealed that Mn(V/VI) oxidized PMSO rapidly *via* oxygen atom transfer to methyl phenyl sulfone ($PMSO_2$), contrasting with the sluggish reaction of Mn(VII) [26]. Fig. 1c showed that PMSO was mostly oxidized to $PMSO_2$ within the first 5 min with both Mn(VII) and Mn(VII)/Mn(II) systems, and completely degraded by the 10^{th} minute, indicating Mn(II) did not enhance Mn(V) and Mn(VI) levels for faster PMSO conversion. Further experimental details on PMSO degradation were provided in Text S2. MeOH, quenching Mn(V) and Mn(VI), reduced their presence [25]. Fig. 1b showed MeOH did not affect SMX elimination, confirming Mn(V) and Mn(VI) insignificance in the Mn(VII)/Mn(II) system for SMX removal.

Recent research highlights the strong oxidative potential of Mn(III) species formed during Mn(VII) decomposition towards various organic pollutants, because of its high redox potential ($E_h = 1.51$ V) [27]. PP can stabilize Mn(III) through complexation, identified by UV–vis spectrum at 256 nm [28]. Mn(III)-PP was synthesized using the method described in Text S1. We also monitored the real-time pH changes of the system after adjusting the pH to 5.0 following the addition of PP (Fig. S6 in Supporting information). An absorption peak was observed at 256 nm in the UV–vis spectrum (Fig. S7a in Supporting information). It was observed that in the Mn(VII)/SMX system, a discernible absorption peak at 256 nm was evident, which significantly intensified upon the introduction of Mn(II) (Figs. S7b and c in Supporting information). Furthermore, to explore the potential involvement of Mn(III) species, PP was introduced into the Mn(VII)/Mn(II) system at varying concentrations. Analysis that followed showed a decrease in the removal effectiveness of SMX by the system (Fig. 1b). This trend underscored the significant influence exerted by PP in complexing Mn(III) species, thereby impacting the degradation of SMX. Mn(III)-PP did not exhibit any degradation of SMX at all three PP concentrations (Fig. S7d in Supporting information). This indicated that the complexation with PP significantly inhibited the oxidative capability of Mn(III) [29]. These observations suggested that intermediate Mn(III) species likely played a pivotal role in mediating the oxidation of SMX.

MnO_2 has an absorption peak at 300–500 nm in UV–vis spectrum [22,30]. Fig. S8a (Supporting information) showed that the Mn(VII)/Mn(II) system exhibits this MnO_2 absorption band, indicating MnO_2 formation. To analyze role of MnO_2, it was synthesized *ex situ*. Fig. 1d showed that MnO_2 alone at 20 μmol/L and 50 μmol/L removed 31.3% and 36.4% of SMX, respectively, indicating oxidative effects. Previous studies attribute the oxidation of MnO_2 primarily to Mn(III) [28]. Fig. S8b (Supporting information) showed Mn(III)-PP peaks when MnO_2 reacted with SMX in the presence of PP. Adding 5 mmol/L PP to the 50 μmol/L MnO_2 system, the degradation of SMX was significantly reduced, unlike the system without PP (Fig. S9 in Supporting information). Thus, Mn(III) likely originated from MnO_2 in the Mn(VII)/Mn(II) system. Fig. 1b showed that PP did not completely prevent SMX degradation, suggesting other mechanisms at play. Fig. 1d demonstrates that adding MnO_2 to the Mn(VII) system significantly enhanced SMX removal, confirming MnO_2 as a catalyst for Mn(VII) activation. Thus, increased SMX degradation with Mn(II) addition was primarily due to the oxidation (mainly from Mn(III)) and catalysis of MnO_2.

Previous studies have indicated that MnO_2 can activate oxidants such as peroxymonosulfate and periodate *via* an interface-catalytic enhancement mechanism [31,32]. Specifically, there exists a potential synergistic interaction between the oxidants and MnO_2, resulting in the surface-activated oxidants exhibiting an elevated oxidation potential. MnO_2 particles before and after the reaction with Mn(VII) were collected for characterization analysis. The chemical state of Mn was explored by XPS (Fig. 2). The Mn 2p spectrum

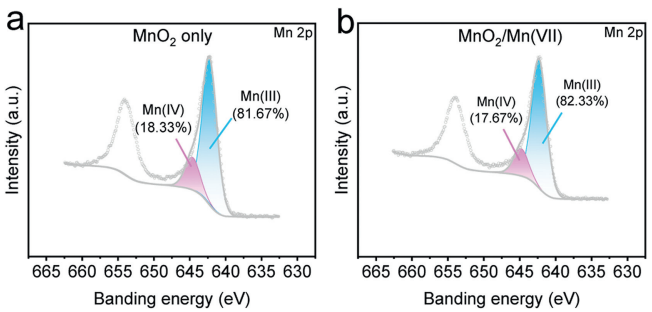

Fig. 2. XPS results of MnO_2 (a) before and (b) after interacting with Mn(VII).

showed a peak at 642.1 eV corresponding to Mn(III) species and a peak at 644.7 eV corresponding to Mn(IV) species. Remarkably, the introduction of Mn(VII) did not significantly alter the Mn(III) to Mn(IV) ratio, indicating limited chemical reactivity between MnO_2 and Mn(VII).

The interaction between MnO_2 and Mn(VII) was further analyzed using Raman spectroscopy. The Mn−O coordination was investigated through Raman spectroscopy, confirming the presence of a surface-activated Mn(VII)* complex at the surface of MnO_2. As illustrated in Fig. 3a, both Mn(VII) and MnO_2 exhibit absorption bands in the range of ~550 cm^{-1} to 680 cm^{-1}, with a prominent peak at 836 cm^{-1} attributed to the stretching vibration of Mn−O bonds [33-35]. At 508 cm^{-1}, Mn(VII) displayed an extra peak attributed to the stretching vibration of O−Mn−O bonds [35], and a feeble peak of 384 cm^{-1} was seen from the bending vibration of Mn−O bonds [36]. Upon mixing MnO_2 with Mn(VII), peaks shifted from 573 cm^{-1} to 579 cm^{-1} (6 cm^{-1}), and the intensity ratio of out-of-plane stretching vibrations altered from the initial $v_1/v_2 = 0.69$ to $v_1/v_2 = 0.59$. A marked decrease in the highest intensity at 836 cm^{-1} was noticed, and the peaks at 508 cm^{-1} and 384 cm^{-1} in the Mn(VII) Raman spectrum were not present in the amalgamated MnO_2 and Mn(VII) system, indicating changes in the coordination environment of Mn−O and O−Mn−O bonds. An inference can be drawn from the above results about the presence of surface-bound Mn(VII)* complexes on the MnO_2 surface. Similar results have also been presented in previous studies [37].

Electrochemical experiments were conducted to further verify the distinction between Mn(VII)* and Mn(VII). As seen in Fig. 3b, open-circuit voltage tests confirmed the role of MnO_2 in augmenting the oxidation potential of Mn(VII), with MnO_2/Pt-Mn(VII)* (0.692 V) being notably higher than Pt-Mn(VII) (0.517 V). Amperometry *i-t* curves further corroborated the open-circuit voltage results. As demonstrated in Fig. 3c, the current signal sharply decreased after the addition of SMX, indicating electron consumption in the solution and electron transfer from SMX to the MnO_2/Pt-Mn(VII)* complex. The weaker current response after adding SMX to the Pt electrode confirmed a less intense redox reaction between Mn(VII) and SMX compared to Mn(VII)* and SMX [38]. To further corroborate the catalytic capabilities exhibited by MnO_2, the EPR spectra were analyzed. As shown in Fig. 3d, the absence of characteristic signals initially indicated that MnO_2 alone was inert in oxidizing DMPO. Conversely, when Mn(VII) was individually analyzed, the characteristic signal of 5,5-dimethyl-2-pyrrolidone-*N*-oxyl (DMPO-X), with a peak intensity ratio of 1:2:1:2:1:2:1, was observed in the EPR spectra. The generation of DMPO-X was primarily due to the oxidation of DMPO by Mn(VII) through an oxygen atom transfer mechanism [39]. When both Mn(VII) and MnO_2 were present, a septet signal appeared with significantly higher peak intensities than when only Mn(VII) was present. The increased peak intensity indicates that MnO_2 enhanced the oxidative capability of Mn(VII) rather than reacting directly with it.

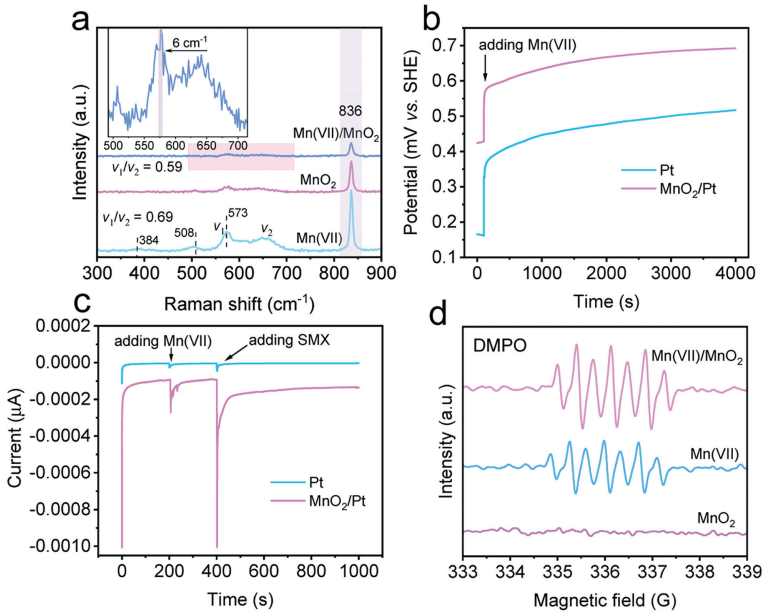

Fig. 3. (a) Raman spectra of the Mn(VII)/MnO_2, Mn(VII), and MnO_2. Experimental conditions: [Mn(VII)] = 0.5 mmol/L, [MnO_2] = 10 mmol/L, pH 5.0. (b) Open-circuit voltage changes on the two surfaces with adding Mn(VII). (c) Instantaneous current changes on the two surfaces with adding Mn(VII) and SMX. (d) EPR spectra of the Mn(VII)/MnO_2, Mn(VII), and MnO_2 systems by using DMPO as a spin-trapping agent. Experimental conditions: [Mn(VII)] = 150 μmol/L, [MnO_2] = 50 μmol/L, 15 μL DMPO.

As shown in Fig. S8c (Supporting information), the UV–vis spectra of the MnO_2 and Mn(VII) mixture show no decrease in the 525 nm peak (characteristic absorbance of Mn(VII)), suggesting that Mn(VII) was not consumed by reacting with MnO_2 [40]. In summary, the collective findings unveil the mechanism of MnO_2 surface activation, wherein the interplay between Mn(VII) and MnO_2 engenders Mn(VII)* species endowed with elevated oxidative potential.

Using UPLC-QTOF-MS/MS in ESI positive mode, 11 major transformation products (TPs) of SMX were detected. Detailed information was in Table S2, Fig. S10 and Fig. S11 (Supporting information). To pinpoint the active sites of SMX, the condensed Fukui index (f^-) was calculated and illustrated in Fig. S12 (Supporting information). The findings indicated that the N13 ($f^- = 0.1889$) with relatively high f^- values, was the most active site of SMX. Using the Fukui index data and the identified products, four degradation pathways for SMX oxidized by Mn(VII)/Mn(II) system were proposed. Fig. 4 proposed four degradation pathways: coupling, amino oxidation, hydroxylation, and bond cleavage. Pathway I: N-centered SMX radicals coupled to form **TP1** ($m/z = 503$), which hydroxylated to **TP2** ($m/z = 519$) [41]. Pathway II: **TP3** ($m/z = 270$), **TP4** ($m/z = 268$), and **TP5** ($m/z = 284$) were hydroxylamine, nitroso, and nitro derivative of SMX, respectively, indicating $-NH_2$ group oxidation. N13 of SMX with the highest f^- value (0.1889) can be oxidized by Mn(VII) to form **TP3**, which oxidized to **TP4** and then **TP5** [42]. Pathway III: at the aniline moiety of benzene ring, **TP6** ($m/z = 255$) was a hydroxylation product of SMX. **TP7** ($m/z = 288$) formed *via* hydroxylation across the C–C bond of isothiazole ring [42]. Pathway IV: S–N bond cleavage formed **TP8** ($m/z = 156$) and **TP9** ($m/z = 99$). C–S bond cleavage yielded **TP10** ($m/z = 94$), which oxidized to **TP11** ($m/z = 108$) [41].

Using the Toxicity Estimation Software Tool (T.E.S.T.), we investigated the toxicological effects of SMX and its degradation intermediates. As shown in Fig. S13 (Supporting information), the evaluation within the Mn(VII)/Mn(II) system revealed insights into the oral toxicity of SMX degradation by-products. Intermediates **TP5**, **TP6**, and **TP10** showed detectable oral toxicity in rats, all lower than the toxicity of SMX. The study found that all degradation products, including SMX, showed no mutagenicity, indicating no genotoxicity. However, most degradation products, except **TP9**, exhibited developmental toxicity at lower levels than SMX. Additionally, the bioaccumulation factors for most products, except **TP6**, were significantly lower than that of SMX, suggesting a reduced tendency to accumulate in organisms. Therefore, degrading SMX using Mn(VII)/Mn(II) is a green and safe approach for pollutants degradation.

This study showed that Mn(II) accelerates the degradation of organic pollutants by Mn(VII), with the rapid breakdown of SMX due to MnO_2 production. *In situ*-generated MnO_2 enabled SMX degradation by Mn(VII) through oxidative and catalytic processes. UV–vis spectra and the addition of PP confirmed the role of MnO_2 in oxidation. The catalytic mechanism involved MnO_2 interacting with Mn(VII) to produce more reactive Mn(VII)* species. SMX degradation by the Mn(VII)/Mn(II) system involved auto-coupling, amino oxidation, hydroxylation, and bond cleavage reactions. T.E.S.T. confirmed reduced cell toxicity of SMX by-products. This paper explores how Mn(II) enhances the oxidation capacity of Mn(VII), offering insights for improving pollutant removal and proposing wastewater treatment methods using Mn(II).

Declaration of competing interest

The authors declare that they have no known competing financial interests or personal relationships that could have appeared to influence the work reported in this paper.

CRediT authorship contribution statement

Haoting Wang: Writing – review & editing, Writing – original draft, Investigation, Data curation. **Mengfan Luo:** Visualization, Validation, Funding acquisition, Conceptualization. **Yuzhong Wang:** Project administration, Methodology. **Jialong Yin:** Methodology, Formal analysis. **Heng Zhang:** Writing – review & editing, Writing – original draft, Methodology, Investigation, Formal analysis. **Jia Zhao:** Writing – review & editing, Methodology, Formal analysis. **Bo Lai:** Visualization, Validation, Supervision, Funding acquisition.

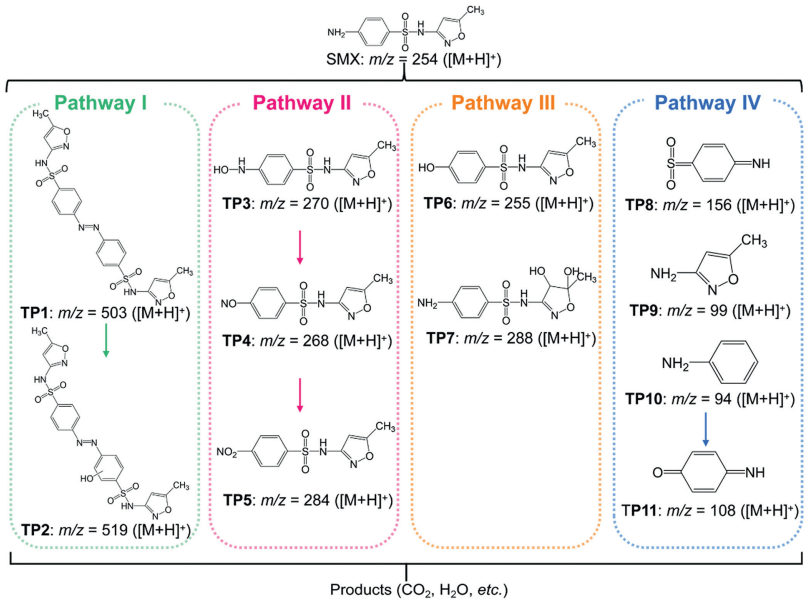

Fig. 4. The degradation pathway of sulfamethoxazole.

Acknowledgments

The authors acknowledge the financial support from the National Natural Science Foundation of China (Nos. 52300102, 523B2094), the Key Laboratory of Jiangxi Province for Persistent Pollutants Prevention Control and Resource Reuse (No. 2023SSY02061), the Natural Science Foundation of Sichuan Province (No. 2024NSFSC0130), and Miaozi Project in Science and Technology Innovation Program of Sichuan Province (No. MZGC20230098).

Supplementary materials

Supplementary material associated with this article can be found, in the online version, at doi:10.1016/j.cclet.2024.110348.

References

[1] A. Mendoza, J. Aceña, S. Pérez, et al., Environ. Res. 140 (2015) 225–241.
[2] P. Verlicchi, M. Al Aukidy, A. Jelic, et al., Sci. Total Environ. 470 (2014) 844–854.
[3] O.M. Rodriguez-Narvaez, J.M. Peralta-Hernandez, A. Goonetilleke, E.R. Bandala, Chem. Eng. J. 323 (2017) 361–380.
[4] J. Li, S.Y. Pang, Z. Wang, et al., Water Res. 203 (2021) 117513.
[5] B.C. Hodges, E.L. Cates, J.H. Kim, Nat. Nanotechnol. 13 (2018) 642–650.
[6] S.S. Xin, B.R. Ma, C.L. Zhang, et al., Appl. Catal. B 294 (2021) 120247.
[7] S.S. Xin, G.C. Liu, X.H. Ma, et al., Appl. Catal. B 280 (2021) 119386.
[8] B. Zhang, X. He, C.Z. Yu, et al., Chin. Chem. Lett. 33 (2022) 1337–1342.
[9] B. Zhang, X. He, X.H. Ma, et al., Sep. Purif. Technol. 247 (2020) 116932.
[10] W. Ren, C. Cheng, P.H. Shao, et al., Environ. Sci. Technol. 56 (2022) 78–97.
[11] L. Peng, X.G. Duan, Y.N. Shang, et al., Appl. Catal. B 287 (2021) 119963.
[12] J. Chen, D.D. Rao, H.Y. Dong, et al., J. Hazard. Mater. 388 (2020) 121735.
[13] J. Jiang, Y. Gao, S.Y. Pang, et al., Environ. Sci. Technol. 49 (2015) 520–528.
[14] P. Yang, K. Wen, K.A. Beyer, et al., Environ. Sci. Technol. 55 (2021) 3419–3429.
[15] J. Jiang, S.Y. Pang, J. Ma, H.L. Liu, Environ. Sci. Technol. 46 (2012) 1774–1781.
[16] Y. Zhou, J.P. Hu, Y. Gao, et al., Chin. Chem. Lett. 33 (2022) 447–451.
[17] J.E. Tobiason, A. Bazilio, J. Goodwill, et al., Curr. Pollut. Rep. 2 (2016) 168–177.
[18] W. Qin, P.Y. Tan, Y. Song, et al., Sep. Purif. Technol. 261 (2021) 118272.
[19] R. Huang, C.T. Guan, Q. Guo, et al., Chin. Chem. Lett. 34 (2023) 107610.
[20] M.J. Frisch, G.W. Trucks, H.B. Schlegel, et al., Gaussian 16 Rev. C.01, Wallingford, CT, 2016.
[21] T. Lu, F.W. Chen, J. Comput. Chem. 33 (2012) 580–592.
[22] K.H. Guo, J.S. Zhang, A.L. Li, et al., Environ. Sci. Technol. Lett. 5 (2018) 750–756.
[23] H.R. Song, L.X. Yan, J. Ma, et al., Water Res. 116 (2017) 182–193.
[24] J. Lu, Y. Zhou, Y.B. Zhou, Chem. Eng. J. 422 (2021) 130126.
[25] J. Chen, B. Sun, Y.T. Zhu, et al., Environ. Sci. Technol. Lett. 9 (2022) 446–451.
[26] Y. Gao, Y. Zhou, S.Y. Pang, et al., Environ. Sci. Technol. 53 (2019) 3689–3696.
[27] S.F. Zhong, H.C. Zhang, Water Res. 148 (2019) 198–207.
[28] S.C. Wang, J. Chen, Y.K. Sun, et al., Environ. Sci. Technol. 57 (2023) 997–1005.
[29] B. Zhang, S.Q. Xia, Z.Y. Wang, et al., Appl. Catal. B 349 (2024) 123861.
[30] A.V. Soldatova, G. Balakrishnan, O.F. Oyerinde, et al., Environ. Sci. Technol. 53 (2019) 4185–4197.
[31] Z.M. Wang, Z.H. Wang, W. Li, et al., Chem. Eng. J. 427 (2022) 130888.
[32] L.W. Yang, F.S. Yang, H. Zhang, et al., J. Hazard. Mater. 454 (2023) 131479.
[33] Z.M. Chan, D.A. Kitchaev, J.N. Weker, et al., Proc. Natl. Acad. Sci. U. S. A. 115 (2018) E5261–E5268.
[34] D. Chen, D. Ding, X. Li, et al., Chem. Mater. 27 (2015) 6608–6619.
[35] M.M. Barsan, I.S. Butler, D.F.R. Gilson, J. Phys. Chem. B 110 (2006) 9291–9297.
[36] T. Gao, M. Glerup, F. Krumeich, et al., J. Phys. Chem. C 112 (2008) 13134–13140.
[37] M.F. Luo, H. Zhang, Y. Ren, et al., Environ. Sci. Technol. (2023) 12847–12857.
[38] J. Liang, X.G. Duan, X.Y. Xu, et al., Environ. Sci. Technol. 55 (2021) 10077–10086.
[39] Y. Zong, Y.F. Shao, W.J. Ji, et al., Chem. Eng. J. 451 (2023) 139106.
[40] M.D. Yu, X.S. He, B.D. Xi, et al., Environ. Sci. Technol. 54 (2020) 10279–10288.
[41] Z.Y. Shi, D.X. Wang, Z.Q. Gao, et al., J. Hazard. Mater. 433 (2022) 128772.
[42] T. Yang, J.M. Mai, H.J. Cheng, et al., Environ. Sci. Technol. 56 (2022) 1221–1232.